

Optical response of plasmonic nanostructures composed of coupled gold nanodisks.

S. Najah, Y. Jarmoumi, A. Akouibaa, S. El Fassi, A. Derouiche and H. Ridouane

Polymer Physics and Critical Phenomena Laboratory. Research Center: Materials and Energy.
Sciences Faculty Ben M'Sik, Hassan II University of Casablanca, P.O. Box 7955, Casablanca, Morocco
E-mail: najahsoukaina.1@gmail.com

Abstract

Due to the coupling effect of Surface Plasmon Resonance (SPR) excited by the incident electromagnetic wave, the gold nanodisks structures show special optical properties that can be applied in many fields of nano-technology. In this work, a model based on the finite element method (FEM) is developed to investigate the effect of the relevant parameters on the optical properties of gold nanodisks. The study is performed for various possible configurations, one, two, three and four gold nanodisks when they are aggregating in dielectric medium. Based on the accurate geometric parameters, we plotted the numerical results of the resonance energy in various conditions involving gap distance and radius of nanoparticles.

Keywords—gold nanodisks, optical properties, surface plasmon resonance and finite element method.

1. Introduction

One of the most interesting properties resulting from the interaction between electromagnetic waves and metallic nanoparticles is the excitation of collective oscillations of the conduction electrons, localized surface plasmon resonances (LSPR). Newly, the physicists seek to control the scattering of an incident optical energy during light-matter interaction, and also, to investigate the features of near-field localization of plasmonic nanoscale configurations. These have significant impacts on development of highly efficient subwavelength optical devices such as biosensors ([1], [2]), photovoltaics and solar cells ([3], [4]), nanoantennas([5], [6]), surface enhanced Raman spectroscopy (SERS) [7], and precise bio/chemical sensors [8]. Self-assembled clusters in numerous simple and complex orientations (include symmetric and antisymmetric regimes) composed of several shapes of noble metallic nanoparticles have broadly been utilized in optic-based applications from sensing to switching ([9], [10]). Gold, silver, copper, and aluminum in dimer ([11], [12]), trimer [13], quadramer [14], heptamer [15], tetramer [16], octamer [17], and oligomers [18] designations are some of the important clusters that have wide-range of utilizations in designing various subwavelength all-optical devices. Furthermore, it's important to study the effect of other parameters such as the size and shape of nanoparticles and the surrounding environment to develop these applications in different devices. From the technical point of view, the quality of formation of Plasmon Resonance in symmetric and antisymmetric structures can be different. Nanospheres ([19], [20] and [21]), nanorods ([22], [23], [24] and [25]), shells and pyramids are some of the popular nanoparticles that can be tailored to support strong plasmon resonance in cluster type aggregates ([11], [14]). Each one of mentioned particles provides specific geometrical features and tunability. Herein, we use the nanodisk particles in designing dimer, trimer and quadramer structures.

Investigating the coupling effect on the optical properties, we determine the quality of appeared plasmon resonant mode.

We utilize an antisymmetric quadrumer cluster of gold nanodisks to make the comparison between the two structures. The Finite Difference Time-Domain FDTD method ([26],[27]), Boundary Integral method ([28], [29]) and the Finite Element FE method ([30],[31]), combined with Monte Carlo simulations are used to study the random and periodic arrangement structures. Moreover, the computer modeling for studying the macroscopic dielectric behavior of multi components condensed phase and layered composite materials ([28], [32] and [33]) are in full progress.

The remainder of the paper is organized as follows: In Section II, we give a brief review of Dielectric Function of Gold. Section III describes the finite element methodology and computational aspects. Section IV reports the results of calculations and comments the effects of interparticle distance d and radius r of gold nanodisks on the (SPR) in symmetric and antisymmetric regimes. Concluding remarks are provided in Section V.

2. Dielectric Function of Gold

The optical response of a metal is quantified by its dielectric constant. The latter is a function of frequency of the interacting electromagnetic wave. Indeed, the interaction of an electromagnetic wave of pulsation, ω , with a metal will lead to a polarization of the medium. This polarization will then generate a change in the complex refractive index, $\tilde{n}(\omega)$, which is related to the dielectric constant by

$$\tilde{n}^2(\omega) = \varepsilon(\omega) \tag{1}$$

In the case of metal nanoparticles, the electronic properties appear when their size is smaller than the mean free path of electrons. From a classical point of view, this corresponds to the fact that the electron-surface collisions are not negligible compared to other interaction processes (electron-electron, electron-phonon) and must be taken into account in the rate of the optical collision of electrons. To well model the interaction of an electromagnetic wave with a Gold nanoparticle, several models are developed to express the dependence of the dielectric constant on wave frequency. Among these, we can quote phenomenological Drude model (DM) ([34], [35], [36] and [37]) and Drude-Lorentz model (DLM) (e.g. [38]). Each has its advantages and weaknesses. The first ignores the interband transitions, while these transitions are possible when the incident photon energy exceeds a certain threshold. DLM best describes the dielectric function of Gold, only in the frequency band between 0.5 eV and 3.5 eV. In order to describe the permittivity of Gold in a wide frequency band, use was made of DM with TCP. This model is valid in the frequency band between 0.5 eV to 6.5 eV, corresponding to wavelengths between 200nm and 2400nm. Within the framework of this model, the permittivity of a Gold nanoparticle is expressed by:

$$\varepsilon = \varepsilon_{\infty} - \frac{\omega_D^2}{\omega^2 + i\gamma\omega} + \sum_{j=1}^2 A_j \Omega_j \left(\frac{e^{i\phi_j}}{\Omega_j - \omega - i\Gamma_j} + \frac{e^{-i\phi_j}}{\Omega_j + \omega + i\Gamma_j} \right) \tag{2}$$

In this relationship, ε_{∞} is the permittivity at infinite frequency, ω_D is the frequency of the volume plasmon, γ is the collision rate of electrons, and the third contribution in the r.h.s of the above relation represents the Lorentz term.

3. Finite element methodology

The dielectric behavior of heterogeneous structures has stimulated many theoretical studies based on numerical calculations, especially in the case where the inclusions are randomly dispersed in the matrix ([39], [40]). For this particular case, the laws governing the dielectric behavior of composite materials are deduced [39]. In order to study some details of the dielectric properties of periodic composites in the quasistatic limit, the finite element method is used to determine the effective permittivity. A detailed description of the method can be found in the literature [41]. Here, we consider a parallel plate capacitor, as shown in figure 1, which is formed by two metal plates of area $S_d = L \times L$ and separated by the height L . The two plates are submitted to a potential difference $(V_2 - V_1)$.

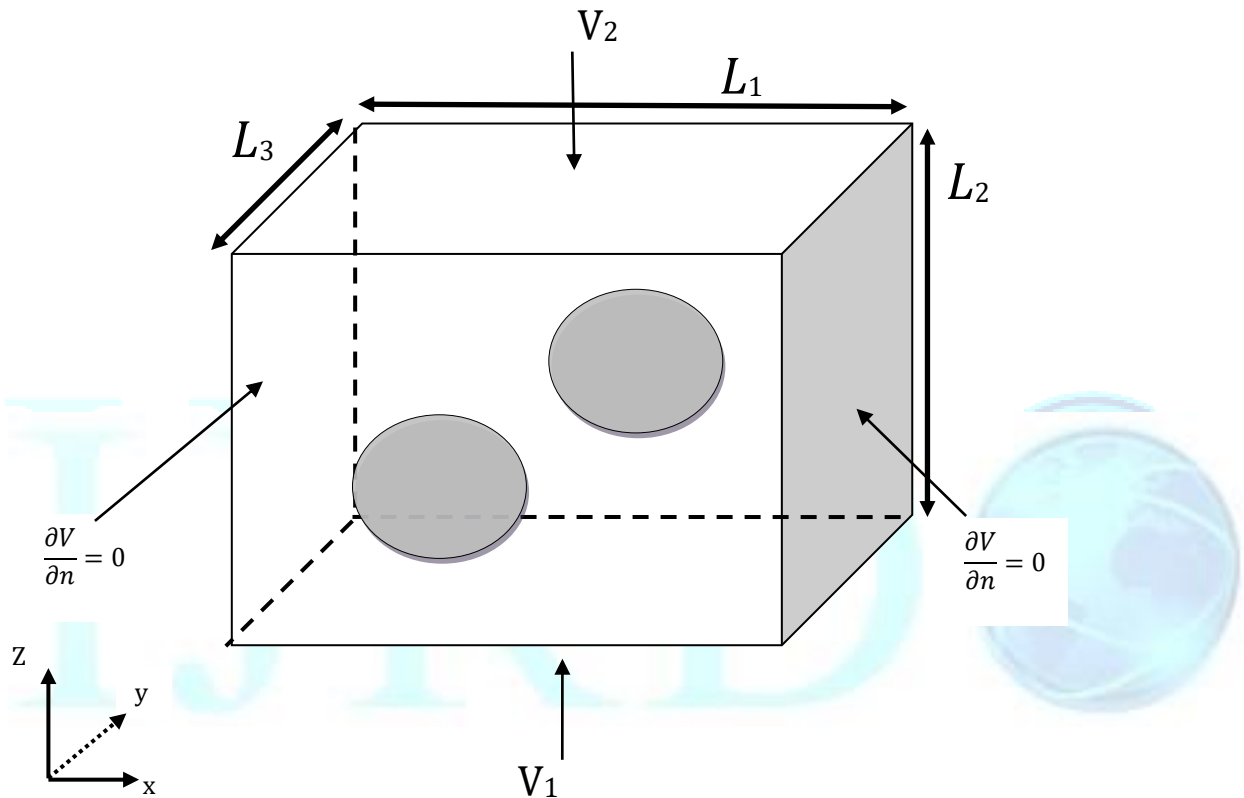


Fig.1: Schematic representation of a three-dimensional composite medium by a cell with length L_1 , width L_2 and height L_3 . This cell contains two gold nanodisks. On the boundary of each cell, the potential is V_1 on the top, and V_2 on the bottom, and its normal derivative $\partial V/\partial n$, is equal to zero along the vertical walls.

Solving the problem at hand means finding the local potential distribution inside the unit cell volume by solving the first principle of electrostatics, namely Laplace’s equation:

$$\nabla(\epsilon_0 \epsilon(r) \nabla V) = 0 \tag{3}$$

Where $\epsilon(r)$ and V are the local relative permittivity and the potential distribution inside the spatial domain respectively, with zero charge density. $\epsilon_0 = 8.85 \cdot 10^{-12} \text{F m}^{-1}$ is the permittivity of the vacuum. The electrostatic energy, W_e^k , and losses, P_e^k , can be expressed in terms of the potential derivatives for each tetrahedral element by:

Journal of Applied Science

$$W_e^k = \frac{\epsilon_0}{2} \iiint \epsilon'_k(x, y, z) \left[\left(\frac{\partial V}{\partial x}\right)^2 + \left(\frac{\partial V}{\partial y}\right)^2 + \left(\frac{\partial V}{\partial z}\right)^2 \right] dv_k \quad (4)$$

$$P_e^k = \frac{\epsilon_0}{2} \iiint \omega \epsilon''_k(x, y, z) \left[\left(\frac{\partial V}{\partial x}\right)^2 + \left(\frac{\partial V}{\partial y}\right)^2 + \left(\frac{\partial V}{\partial z}\right)^2 \right] dv_k \quad (5)$$

Here, ϵ_k and V_k represent the permittivity and the volume of the k^{th} tetrahedron element, respectively. The phases of the composite are described through their complex permittivity $\epsilon_k = \epsilon'_k + i\epsilon''_k$. Periodic boundary conditions $\partial V/\partial n = 0$ are enforced on faces perpendicular to x and y space-directions. Consequently, the edge fringing effects can be eliminated, and then, the effective permittivity of the composite can be determined from energy W_e^k and losses P_e^k stored in the capacitor according to

$$W_e = \frac{1}{2} \epsilon'_{eff} \frac{S_d}{L} (V_2 - V_1)^2 \quad (6)$$

$$P_e = \frac{1}{2} \omega \epsilon''_{eff} \frac{S_d}{L} (V_2 - V_1)^2 \quad (7)$$

Having established the mathematical equation (3) that describes physics, we must point-out how to solve it for the interested domain, with appropriate boundary conditions. In the frame work of FEM, the domain is decomposed into a number of uniform or non-uniform finite elements that are connected via nodes. For each sub space element, the function modeling the potential V is defined by a polynomial interpolation function. Then, the boundary values are replaced with an equivalent integral formulation. The interpolation polynomials are then replaced into the integral equation and integrated in the interested domain. Then the results of this step are converted into matrix equation, which is afterward solved for V ([41], [42]).

Absorption-cross-section

From the evolution of the effective complex dielectric function, depending on the wavelength (or frequency) of the incident field, the resonance modes that may occur in nanoparticles are identified. For this, it would be interesting to calculate the scattering cross-sections and absorption. The sum of these two quantities defines the extinction cross-section:

$$\sigma_{ext} = \sigma_{abs} + \sigma_{diff} \quad (8)$$

In the case where the dimensions are very small compared to the wavelength, the light scattering can be ignored, and we have: $\sigma_{ext} \approx \sigma_{abs}$

The cross-section of extinction (absorption) can be determined from the imaginary part of the effective dielectric function of the composite using the following equation [43]

$$\sigma_{abs} = \frac{v_p}{f} \frac{k}{n_{eff}} \epsilon''_{eff} \quad (9)$$

Here, v_p stands for the common volume of nanoparticles, f is their fraction, k is the wave-vector amplitude of the electromagnetic wave, and n_{eff} represents the refractive index that can be related to the real and imaginary parts, ϵ'_{eff} and ϵ''_{eff} of the effective permittivity by ([44]).

Journal of Applied Science

$$n_{eff} = \left(\frac{\sqrt{\epsilon'_{eff}{}^2 + \epsilon''_{eff}{}^2} + \epsilon'_{eff}}{2} \right)^{1/2} \quad (10)$$

This formula clearly shows that the peak of $\text{Im}(\epsilon_{eff})$ indicates that the light is rather absorbed in specific regions. The effective dielectric function and the effective refractive index are calculated using FEM. Hence, the section of optical absorption is easily obtained. In the following section, we present and discuss our findings.

4. Results and discussion

The plasmonic nanostructures discussed in this work are depicted in Figure 2. Six structures of gold nanodisks are studied and analyzed quantitatively. The first structure (system a) is a single nanodisk (Figure 2a). The other structures are coupled nanodisks for various configurations, dimer, trimer and quadramer (Figures 2 b-f).

In the first case, we study the optical response of a single gold nanodisk, whose results are compared to those of a single gold nanosphere of same radius. The disk radius and height are $r=14$ nm and $h=5$ nm, respectively. The particles are immersed in cubic matrix of permittivity $\epsilon = 1.77$ (fixed for the entire following studies) and a volume fraction of $f=0.05$.

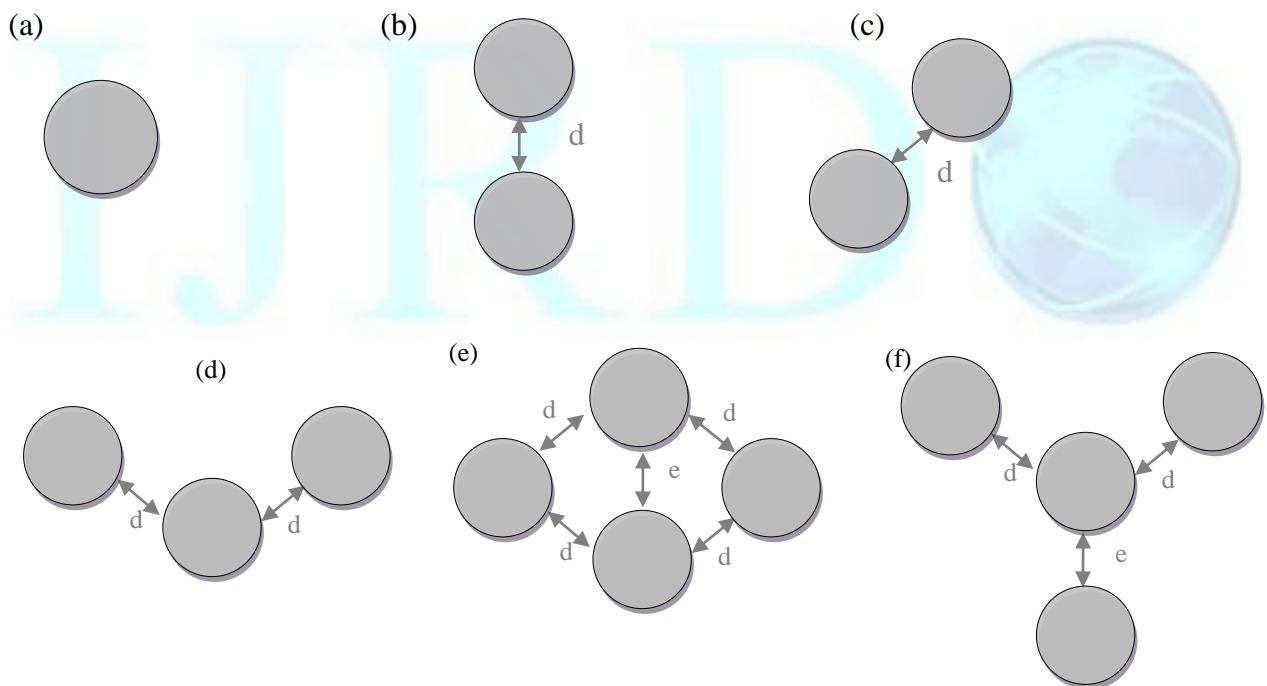


Fig.2: Schematic representation of the different configurations of gold nanodisks.

Figure 3 compares the optical response of these single particles (nanodisk, sphere). In particular, we plot the variation of the real and imaginary parts of the effective permittivity as a function of the photon energy. We recall that the external electric field is applied in the z-direction. The imaginary part of the effective permittivity $\text{Im}(\epsilon_{eff})$ permits to obtain the peak position of the Plasmon Resonance. This peak is shown at the photon energy $E_R = 1.97$ eV

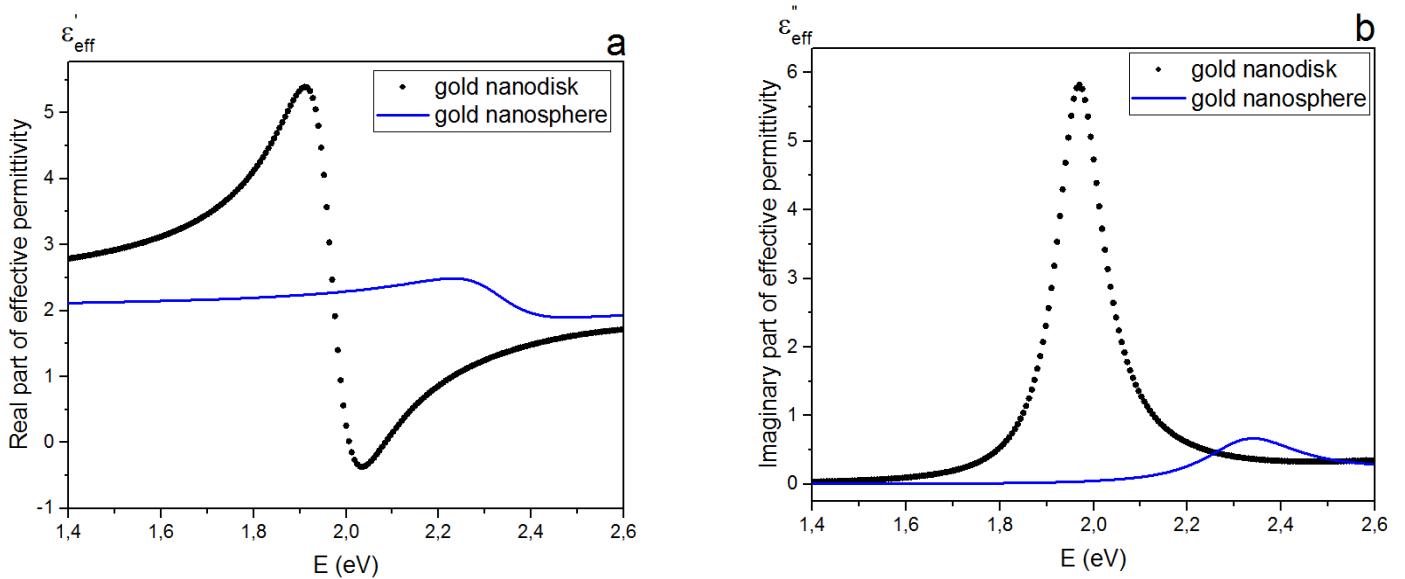


Fig.3: Evolution of the real part (a) and imaginary part (b) of the effective permittivity for gold nanodisk and nanosphere. The disk radius is 14 nm and the height is 5 nm (black curve). The gold nanosphere has the same radius (blue curve). The particles are immersed in cubic matrix of permittivity $\epsilon = 1.77$.

(Wavelength $\lambda \sim 631\text{nm}$) for the disk and $E_R = 2.36\text{ eV}$ (Wavelength $\lambda \sim 526\text{nm}$) for the sphere (with same radius).

In the second case, we examine the coupling effect on the optical property in different modes. For this, we consider two configurations which contain two couples of gold disks, which in the first configuration are located in the longitudinal mode (Figure 2b) and in randomly oriented mode (Figure 2c) in the second one. It should be noted that we keep the same previous values of the radius of the gold nanodisks, the height, and the volume fraction of $f = 0.05$.

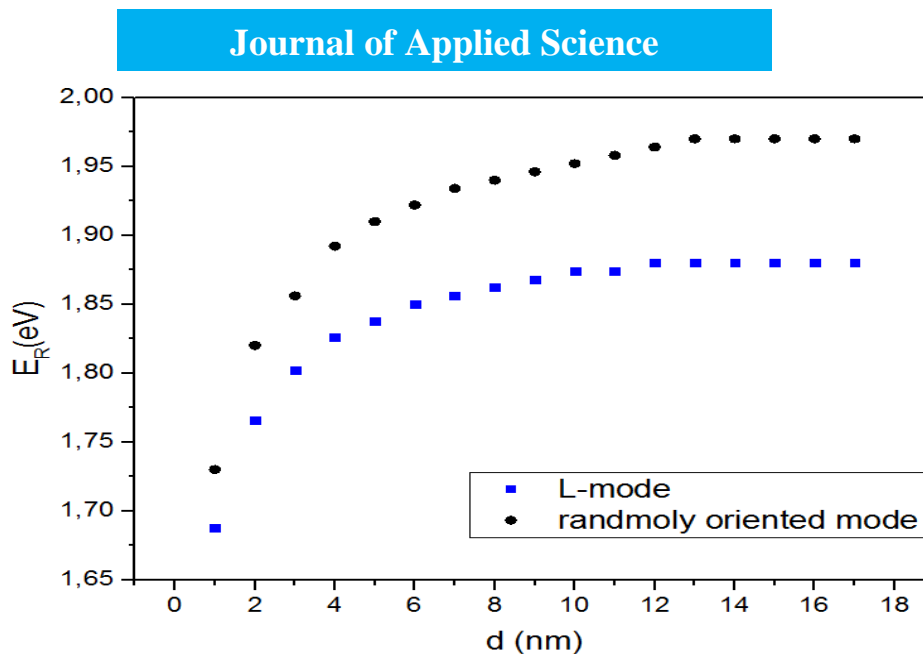


Fig.4: Evolution of the resonance energy in term of the gap distance. The value of the gap distance increases from 1nm to 18nm. The disk radius and height are 14 nm and 5 nm respectively.

The corresponding results have been well shown in the figure4. report the evolution of the resonance energy in term of the gap distanced by changing this from 1nm to 18nm. Three salient features can be observed. On the one hand, when the gap distance increases, we observe an increase of the resonance energy. On the other hand, when the gap distance reaches the value of 14 nm (almost equal the radius of the disk), the resonance energy is kept fixed. Otherwise, when we compare the both modes, we observe that the L-mode gives resonance energy values reaching IR interval.

Now, we study the coupling effect in the subgroup v-shaped (figure 2d). For this, we keep r, h and f of disks parameters fixed. The results are depicted in figure 5; we then plot the absorbing cross-sectional profiles for the subgroup versus the gap distance. Noticing in this diagram that for gap distances smaller than 4 nm, the energy of multipolar modes is strong, this indicates the quality of appeared second peak. For bigger sizes of gap distances, the energy of multipolar peak is dramatically weak, and even this peak is absent for d=8 nm. These results show that the weak coupling gives rise to blue-shift, due to decrement the intensity of multipolar extremes.

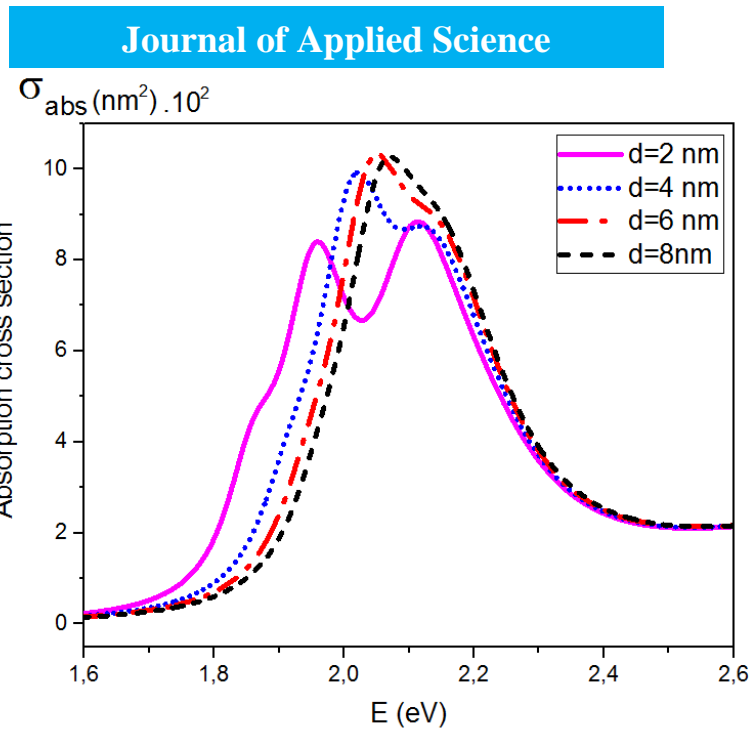


Fig. 5: Absorption Spectrum of subgroup v-shaped composed of gold nanodisks, with the radius of $r=14\text{nm}$ and the heights $h=5\text{nm}$. The value of the gap distance increase from 2nm to 8nm .

In continue, we study coupling effect for a symmetric quadrumer composed of gold nanodisks (figure2 e), the nanoparticles are located with two different gap distances from each other ($d=4\text{ nm}$, $e=3\text{ nm}$), so the system is in a strong coupling configuration. Two situations are examined depending on the external electric field direction. The latter is applied in two opposite linear polarizations (transverse and longitudinal modes). For each mode we sketched the absorbing cross-sectional profiles (figure 6 a, b). Beginning by the longitudinal one and increasing the radius of gold nanodisks, in the examined quadrumer, from $r=14\text{ nm}$ to $r=16\text{ nm}$ (corresponding to the change of the volume fraction from 5% to 6%), we remark that this gives rise to dramatic red-shifts in the localization of SPR peak. For instance, for $r=14\text{ nm}$, the peak of dipolar electric mode appears at $\lambda\sim 701\text{nm}$. In the same condition, for a quadrumer composed of nanodisks with the radius $r= 16\text{ nm}$, the SPR peak position appears at $\lambda\sim 730\text{nm}$. For the incident transverse polarization mode, the structure reflects the same

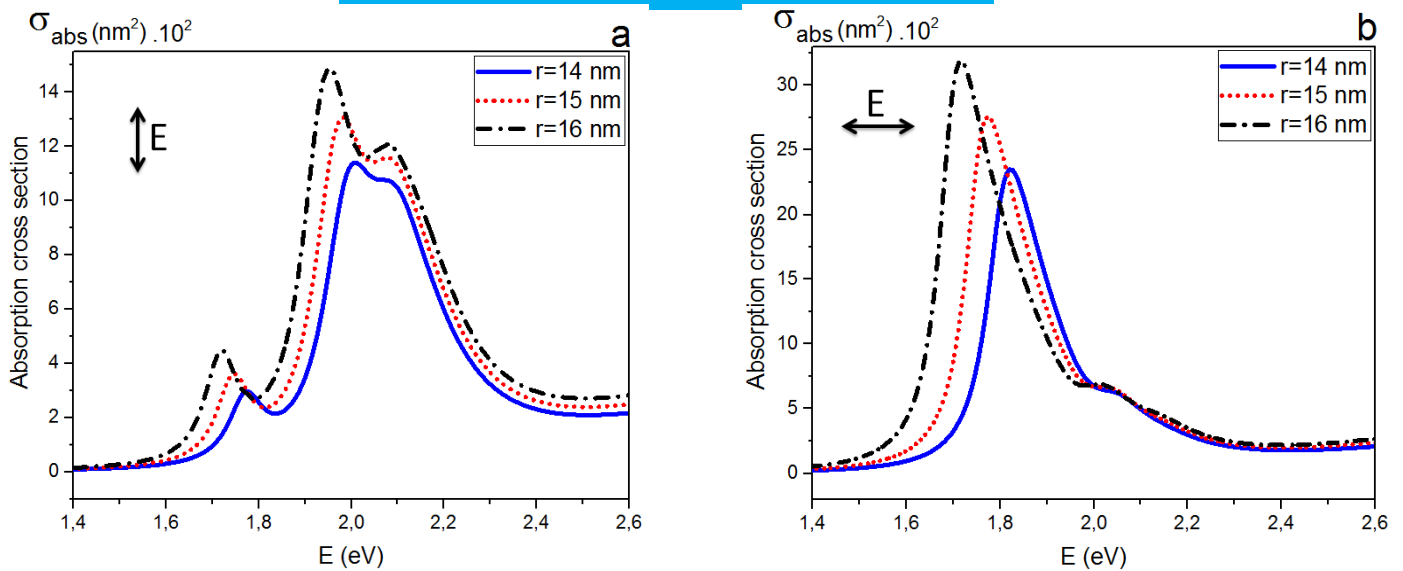


Fig. 6: Absorption Spectrum of The symmetric quadrumer, for various nanodisks radius with fixed height $h=5\text{nm}$, under illumination by longitudinal (a) and transverse (b) electric polarization modes. The particles are immersed in a cubic matrix of permittivity $\varepsilon=1.77$.

behavior as for the longitudinal one, where the SPR peak is also red shifted but the absorption cross-section is more pronounced than for longitudinal mode. The important remark is that for the bigger sizes of the quadrumer, strong plasmon resonant modes can be supported effectively, but it should be considered that more increments in the size of nanoparticles cause undesired absorption of electromagnetic (EM) field by the structure.

As mentioned in the previous paragraph, the size of radius of nanoparticles is important for determining the SRP peak position. Other structure studied here is the antisymmetric nanocluster, depicted in (figure.2 f), which is based on the same geometrical parameters. The result is shown in figure 7; the radius of the gold disks is increasing in the range of 14-16 nm.

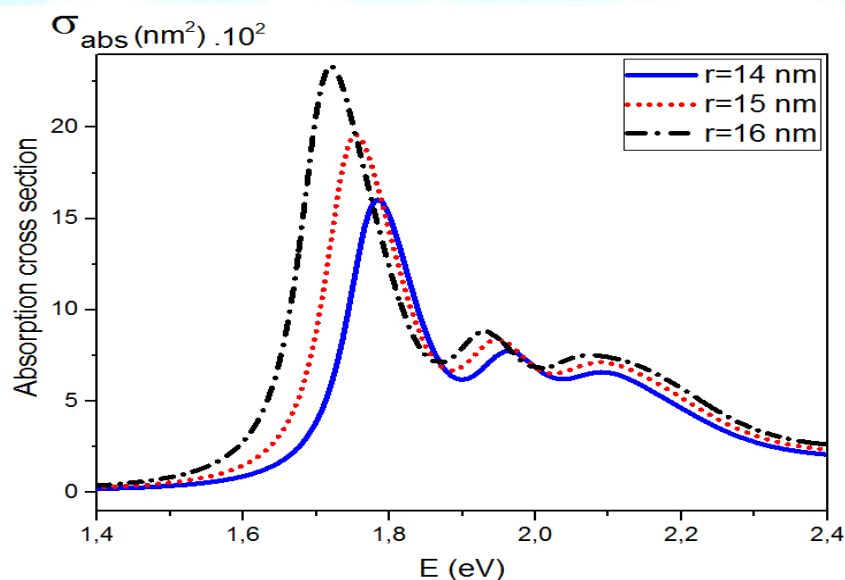


Fig.7: Absorption Spectrum of The antisymmetric quadrumer for various nanodisks radius from 14nm to 16nm and with fixed height $h= 5\text{nm}$ under illuminating by longitudinal electric polarization mode. The particles are immersed in cubic matrix of permittivity $\varepsilon=1.77$.

For $r=14$ nm and $r=16$ nm, we observed the peak positions at $\lambda \sim 112$ nm and $\lambda \sim 116$ nm respectively, we see that whenever we increased the radius of inclusions, the structure gives rise to dramatic red-shifts in the position of the quadrupole and dipole peaks.

5. Conclusions

In this work, we examined optical properties of different nanoclusters, which are composed of gold nanodisks. All the nanostructures are considered in water ($\epsilon = 1.77$). Choosing accurate geometrical sizes for a well-organized nanodisks, the effect of structural modifications on the spectral response of the heterogenic structures has been examined numerically. It is shown that increasing the size of nanodisks radius gives rise to red-shift of the SPR-peak. Increasing and decreasing the size of gap distance between proximal nanoparticles of subgroup v-shaped arrangements causes blue and red shifting of the SPR-peak and resembles the weak and strong coupling regimes, respectively. Comparing between the symmetric and antisymmetric quadrumer cluster of gold nanodisks, the two structures reflect the same response, where the SPR-peak shifts toward the red. These structures have a strong potential to employ in various applications such as sensing, biological imaging, optical and optoelectronic devices and cancer therapy.

Acknowledgments

We are much indebted to Professor M. Benhamou for helpful discussions and useful remarks. Also, we express sincere appreciation and deep gratitude to all participants in this work for especially to Dr. A. Maarouf and Dr. K. El Hasnaoui.

6. References

- [1] G.J.Nusz, A.C.Curry, S.M.Marinakos, A.Wax, and A.Chilkoti, "Rational selection of gold nanorod geometry for label-free plasmonic biosensors," ACS Nano, vol. 3, no. 4, pp. 795–806, Mar. 2009.
- [2] A. G. Brolo, "Plasmonics for future biosensors," Nature Photon, vol.6, pp. 709–713, Nov. 2012
- [3] Y. Yang, S. Pillai, H. Mehrvarz, and M. A. Green, "Plasmonic degradation and the importance of over-coating metal nanoparticles for a plasmonic solar cell," Solar Energy Mater. Solar Cells, vol. 122, pp. 208–216, Mar. 2014.
- [4] J. Park, N. Park, and S. Varlamov, "Optimum surface condition for plasmonic Ag nanoparticles in polycrystalline silicon thin film solar cells," Appl. Phys. Lett., vol. 104, no. 3, p. 033903, Jan. 2014.
- [5] F. Neubrech, A. Pucci, T. W. Cornelius, S. Karim, A. García-Etxarri, and J. Aizpurua, "Resonant plasmonic and vibrational coupling in a tailored nanoantenna for infrared direction," Phys.Rev.Lett., vol. 101, p. 157403, Oct. 2008.
- [6] N. Zhang et al., "High sensitivity molecule detection by plasmonic nanoantennas with selective binding at electromagnetic hotspots," Nanoscale, vol. 6, no. 3, pp. 1416–1422, Oct. 2014.
- [7] A. Ahmadvand and S. Golmohammadi, "Optimized plasmonic configurations: Adjacent and merging regimes between a symmetric couple of Au rod/shell nano-arrangements for LSPR sensing and spectroscopic purposes," J. Nanoparticle Res., vol. 16, no. 7, p. 2491, Jun. 2014.
- [8] F. Hao, Y. Sonnefraud, P. Van Dorpe, S. A. Maier, N. J. Halas, and P. Nordlander, "Symmetry breaking in plasmonic nanocavities: Subradiant LSPR sensing and a tunable Fano resonance," Nano Lett., vol. 8, no. 11, pp. 3983–3988, Oct. 2008.

- [9] Z. Nie, A. Petukhova, and E. Kumacheva, "Properties and emerging applications of self-assembled structures made from inorganic nanoparticles," *Nature Nanotechnol.*, vol. 5, no. 1, pp. 15–25, Dec. 2010.
- [10] J. A. Fan et al., "Self-assembled plasmonic nanoparticle clusters," *Science*, vol. 328, no. 5982, pp. 1135–1138, May 2010.
- [11] J. B. Lassiter et al., "Close encounters between two nanoshells," *Nano Lett.*, vol. 8, no. 4, pp. 1212–1218, 2008.
- [12] L. Cheng, J. Song, J. Yin, and H. Duan, "Self-assembled plasmonic dimers of amphiphilic gold nanocrystals," *J. Phys. Chem. Lett.*, vol. 2, no. 17, pp. 2258–2262, Aug. 2011.
- [13] P. K. Jain and M. A. El-Sayed, "Surface plasmon coupling and its universal size scaling in metal nanostructures of complex geometry: Elongated particle pairs and nanosphere trimers," *J. Phys. Chem. C*, vol. 112, no. 13, pp. 4954–4960, Mar. 2008.
- [14] J. A. Fan et al., "Fano-like interference in self-assembled plasmonic quadrumer clusters," *Nano Lett.*, vol. 10, no. 11, pp. 4680–4685, Oct. 2010.
- [15] J. A. Fan et al., "Plasmonic mode engineering with templated self-assembled nanoclusters," *Nano Lett.*, vol. 12, no. 10, pp. 5318–5324, Sep. 2012.
- [16] Z. Fan, H. Zhang, and A. O. Govorov, "Optical properties of chiral plasmonic tetramers: Circular dichroism and multipole effects," *J. Phys. Chem. C*, vol. 117, no. 28, pp. 14770–14777, Jun. 2013.
- [17] B. Luk'yanchuk et al., "The Fano resonance in plasmonic nanostructures and metamaterials," *Nature Mater.*, vol. 9, pp. 707–715, Aug. 2010.
- [18] B. Hopkins, A. N. Poddubny, A. E. Miroshnichenko, and Y. S. Kivshar, "Revisiting the physics of Fano resonances for nanoparticle oligomers," *Phys. Rev. A*, vol. 88, pp. 053819-1–053819-10, Nov. 2013.
- [19] A. Akouibaâ, M. Benhamou, A. Derouiche, F. Benzouine, H. Ridouane, A.R. Senoudi, A. Boussaid, "Numerical study of the plasmonic resonance of multi-phases nanoparticles," *Inter. Jour. Aca. Res*, vol. 4, no. 6, p. 213, Nov. 2012.
- [20] A. Ouari1, M. Benhamou, A. Akouibaa, A. Derouiche, A.R. Senoudi, A. Boussaid, "Numerical study of the optical properties of core-shell bimetallic nanospheres gold-gold and gold-silver : Comparison to experiment," *Inter. Jour. Aca. Res*, vol. 5, no. 4, pp 53-69 July. 2013.
- [21] A. Akouibaâ, A. Derouiche, H. Ridouane, A. Bettachy, F. Benzouine, "Numerical Study of Optical Properties of Tow Assembled GoldCore/Polymer-Shell Nanoparticles in Dielectric Medium", *Inter. Jour. Adv. Res. Comp. Sc. Soft. Eng*, vol. 4, p. 273, July. 2014.
- [22] A. Akouibaâ, M. Benhamou, A. Derouiche, "Simulation of the Optical Properties of Gold Nanorods: Comparison to Experiment," *Inter. Jour. Adv. Res. Comp. Sc. Soft. Eng*, vol. 3, p. 657, Sep. 2013.
- [23] A. Akouibaâ, A. Derouiche, H. Ridouane, S. El Fassi, "Numerical investigation of surface plasmon resonance of gold nanorod dimers and trimers in dielectric medium", *Inter. Jour. Emerg. Res. Mange. Tech*, vol. 3, p. 102, Nov. 2014.
- [24] A. Akouibaâ, A. Derouiche, H. Ridouane, "Numerical study of the effects of polymeric shell on plasmonic resonance of gold nanorods", *Inter. Jour. Comp. Mat. Sc. Eng*, vol. 3, p. 1450024, Dec. 2014.
- [25] Z. Bassam, A. Akouibaa, A. Derouiche, S. El-fassi, "Numerical Study of the Polarization Direction Effect on the Optical Properties of Gold Nanorods in Dielectric Medium", *Inter. Jour. Adv. Res. Comp. Sc. Soft. Eng*, vol. 5, p. 160, Dec. 2015.
- [26] O. Pekonen, K. Kärkkäinen, A. Sihvola, K. Nikoskinen, "Numerical testing of dielectric mixing rules by FDTD method", *J. Electromagn. Waves Applicat.* 13 (1999) 67e87.
- [27] K. Kärkkäinen, A. Sihvola, K. Nikoskinen, "Effective permittivity of mixtures: numerical validation by the FDTD method", *IEEE Trans. Geosci. Remote Sensing* 38 (2000) 1303e1308.

- [28] C. Brousseau, A. Beroual, "Effective permittivity of composites with stratified particles", *J. Phys. D* 34 (2001) 704e710.
- [29] B. Sareni, L. Krähenbühl, A. Beroual, A. Nicols, "A boundary integral equation method for the calculation of the effective permittivity of periodic composites", *IEEE Trans. Mag.* 33 (2) (1997) 1580e1583.
- [30] Chen Ang, Zhi Yu, RuyanGuo, A.S. Bhalla, "Calculation of dielectric constant and loss of two-phase composites", *J. Appl. Phys.* 93 (6) (2003) 3475e3480.
- [31] A. Mejdoubi, C. Brosseau, "Finite-element simulation of the depolarization factor of arbitrarily shaped inclusions", *Phys. Rev. E* 74 (3) (2006) 031405.
- [32] L.F. Chen, C.K. Ong, B.T.G. Tan, C.R. Deng, "Effective permittivity of layered dielectric sphere composites", *J. Mat. Sc.* 33 (1998) 5891e5894.
- [33] X. Liu, Y. Wu, R. Li, Z. Zhang, "Effect of interphase on effective permittivity of composites", *S. J. Phys. D* 44 (2011) 115402.
- [34] C. Kittel, *Introduction to Solid State Physics*, Wiley, New York, 1956.
- [35] U. Kreibig and L. Genzel, "Optical absorption of small metallic particles," *Surf. Sci.*, vol. 156, pp. 678-700, 1985.
- [36] R. Kubo, A. Kawabata and S. Kobayashi, "Electronic Properties of Small Particles," *Ann. Rev. Mater.Sci.*, vol. 14, pp. 49-66, 1984.
- [37] G. Weick, R.A. Molina, D. Weinmann and R.A. Jalabert, "Lifetime of the first and second collective excitations in metallic nanoparticles," *Phys. Rev. B*, vol. 72, pp. 115410(1-17), 2005.
- [38] A Vial and T. Laroche, "Description of dispersion properties of metals by mean of the critical points model and application to the study of resonant structures using the FDTD method," *J. Phys. D: Appl. Phys.*, vol. 40, pp. 71527158, 2007.
- [39] K. Kärkkäinen, A. Sihvola, K. Nikoskinen, "Analysis of a three-dimensional dielectric mixture with finite difference method", *IEEE Trans. Geosci.Remote Sensing* 39 (5) (2001) 1013e1018.
- [40] V. Myroshnychenko, C. Brosseau, "Finite-element modeling method for the prediction of the complex effective permittivity of two-phase random statistically isotropic heterostructures", *J. Appl. Phys.* 97 (4) (2005) 044101.
- [41] V. Myroshnychenko, C. Brosseau, "Finite-element method for calculation of the effective permittivity of random inhomogeneous media", *Phys. Rev. E* 71 (2005) 016701.
- [42] A. Mejdoubi, C. Brosseau, "Finite-element simulation of the depolarization factor of arbitrarily shaped inclusions", *Phys. Rev. E* 74 (3) (2006) 031405.
- [43] G. Weick, R.A. Molina, D. Weinmann and R.A. Jalabert, "Lifetime of the first and second collective excitations in metallic nanoparticles," *Phys. Rev. B*, vol. 72, pp. 115410-1-17, 2005.
- [44] E.D. Palik, *Handbook of Optical Constants of Solids III*, Academic Press, New York, 1991.